Proceedings of the Society of Photo-optical Instrumentation Engineers

Volume 194

Applications of Optical Coherence

William H. Carter
Editor

August 29-30, 1979,

Proceedings of the Society of Photo-Optical Instrumentation Engineers

Volume 194

Applications of Optical Coherence

August 29-30, 1979
San Diego, California

William H. Carter
Naval Research Laboratory
Editor

ISBN 0-89252-222-4

Printed in the United States of America.

APPLICATIONS OF OPTICAL COHERENCE

Volume 194

INTRODUCTION

William H. Carter
Naval Research Laboratory
Washington, D. C.

The theory of partial coherence describes the effects of random time fluctuations of a light field on the intensity observed by eye or photodetector. It is very well known that light from a laser behaves differently from the light from a thermal source because it is "coherent." However, it is not so well known except by specialists that thermal light also exhibits coherence phenomena. This becomes particularly evident in the operation of a microscope, of an interferometer, and of many related instruments. The theory of partial coherence is more than an academic exercise. It is in fact a very useful tool for instrument design and for the analysis of some useful optical phenomena. I have tried to show this by the choice of papers selected for this seminar.

In this seminar papers were presented which demonstrate some useful application of the theory of partial coherence or the coherence phenomena it describes. Session 1 includes papers dealing with the use of this theory in the design and operation of optical instruments and in a reformulation of the classical theory of radiometry to properly describe the effects of interference. Session 2 contains papers of a somewhat different nature. Here the theory is used to study the effects on a light beam due to propagation through a turbulent medium and to study the phenomena of speckle. In particular, Professor Goodman in the opening paper of this session discusses the similarities and differences between the theory of speckle and the theory of partial coherence from which it was derived. The final session includes a collection of papers discussing some new techniques involving optical coherence which serve to emphasize a wide range of useful applications.

Presently the theory of partial coherence is not well known nor much used except by a rather small group, most of whom are not engineers. It is my hope that greater emphasis will be given in the training of optical engineers in the use of the theory for solving practical problems.

APPLICATIONS OF OPTICAL COHERENCE

Volume 194

Contents

APPLICATIONS OF OPTICAL COHERENCE

Volume 194

SESSION 1

INSTRUMENTS AND RADIOMETRY

Chairman
William H. Carter
Naval Research Laboratory

Review of optical coherence effects in instrument design

George O. Reynolds
Arthur D. Little, Inc.
Cambridge, Massachusetts 02140

and

John B. DeVelis
Merrimack College
Physics Department
North Andover, Massachusetts 01845

Abstract

Improved performance in many optical instruments has been achieved by considering coherence effects in the design of the optical instrument. In this paper such improvements are reviewed by heuristically describing the fundamental principles of partial coherence which are required in the design of such instruments. Furthermore, these coherence effects, which arise from both coherent and incoherent sources of radiation, are illustrated by discussing a selected set of instruments in which improved performance has been achieved. These examples include high-resolution recording and analyzing instruments which use incoherent sources, as well as imaging and mensuration instruments which use coherent sources. A set of guidelines for determining when coherence effects influence system performance with respect to linearity, resolution and noise is also presented.

Introduction

The time period prior to the experimental discovery of the laser witnessed the theoretical development and experimental verification of classical coherence theory, as well as the application of communication and information theory concepts, in the design of optical systems. Communication techniques applied to optical systems led to the introduction of the optical transfer function as a viable tool in the design and analysis of incoherent optical imaging systems. The work in coherence theory was primarily concerned with the propagation of radiation. However, application of this theory to the imaging problem determined the parameters and conditions of coherence for which the optical system is linear.

The advent of the laser stimulated considerable research using a coherent optical source. In imaging systems equipped with laser sources, researchers observed deleterious effects in the image, such as edge ringing, edge shifting, and the presence of speckle noise. Simultaneously, the long coherence length of the laser led to a rebirth of holography, since improved three-dimensional imaging effects were observed. The subsequent use of holograms as filters also revived interest in optical data processing.

The incoherent and coherent limits of the theory of partial coherence were utilized to describe these various incoherent and coherent imaging phenomena. Techniques for linearizing the coherent imaging system and reducing the effect of speckle noise were also developed.

In addition, interest in high-resolution optical analyzing instruments led to the examination of the partially coherent imaging problem. This resulted in a generalized treatment of the problem in which it was shown that optical imaging systems become nonlinear when the degree of spatial coherence in the object plane becomes comparable in size to the resolved object. Techniques for avoiding these system nonlinearities were subsequently developed.

In this paper, we review the effects of optical coherence in instrument design by first describing the necessary elements of classical coherence theory from an experimental viewpoint. We treat spatial and temporal coherence effects separately, and then review those aspects of the theory of partial coherence which are important in the design of optical instruments.

For spatial coherence, this approach results in a relationship between conditions for coherence of the radiation and optical system parameters which define the operating region of linearity for any optical system. These effects are explored in a variety of instruments and result in general guidelines useful in instrument design.

We treat coherent imaging problems separately and show that the introduction of partial coherence tends to degrade such systems. We also treat design considerations for optimizing the degree of partial coherence in such systems in a series of examples.

Finally, we discuss the effects of temporal coherence and illustrate how its control optimizes system performance using some examples. The results outlined in this paper should be useful in optimizing the coherence effects in designing optical instruments.

Elements of classical coherence theory

In this section, we describe a heuristic and experimental approach to the subject of classical coherence theory.* The theory of partial coherence is an appropriate starting point from which the formulations of the imaging problem can be developed.[3] However, we have

*A rigorous description of this theory is available in the published literature.[1,2]

restricted our discussions to those elements of the theory which are essential to the investigation of coherence effects in instrument design. Examples of instruments in which coherence effects influence the instrument performance are high-resolution instruments, such as microscopes, microdensitometers, contact and projection printers, as well as holographic and other instruments that use laser sources.

The meaning of the terms coherent radiation field and incoherent radiation field is often sought. The definition usually given is that coherent light interferes or diffracts and that incoherent light does not. For this reason, we think of the sun as an incoherent source because we do not normally observe diffraction effects in our every day observations. However, it is a simple matter to demonstrate that this naive explanation is deficient. Such an experiment was first performed by Verdet in 1869.[4] In repeating this experiment two small pinholes, spaced a distance "d" apart, are placed in front of the human eyeball to create a Young's two-point interferometer. The restrictions in the experiment are that the size of the pinhole must be several times larger than the average wavelength of the radiation, and that the distance of the observation plane from the pinholes must be large compared to the pinhole size. When this interferometer is used to observe the sun and the separation of the pinholes is on the order of 100 μm, interference fringes appear. For pinhole separations less than 100 μm, the fringe contrast increases. Figure 1 is a schematic of the experimental arrangement.

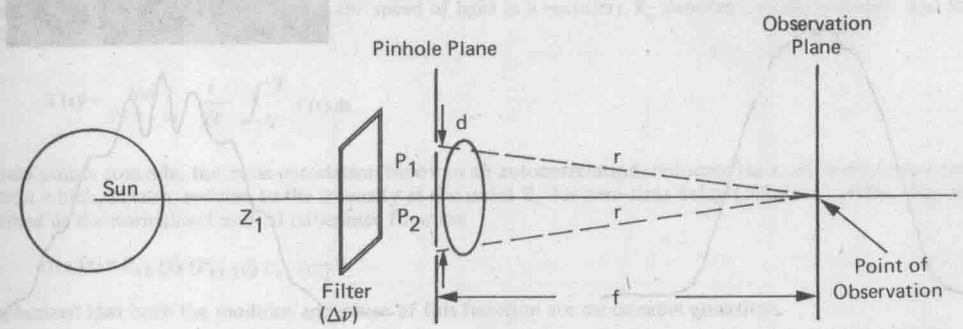

Figure 1 Schematic arrangement of two-pinhole experiment for observing interference fringes with sunlight.

Figures 2-4 show the observed radiation fields and their corresponding microdensitometer traces when the pinhole separations, d, are 50 and 100 μm. Figure 2 shows the intensity distribution in the observation plane and its microdensitometer trace, with a pinhole separation, d, equal to 100 μm. In this case, we see the superposition of two circular diffraction patterns modified by fringes occurring as a result of the interference between the radiation fields from the pinholes. Figure 3 shows the intensity distribution in the observation plane with its accompanying microdensitometer trace for a pinhole separation of 50 μm. We observe interference fringes of higher contrast due to the smaller separation between the pinholes. We repeated the experiment with a spectral filter placed over the pinholes to reduce the spectral bandwidth of the radiation to approximately 50 Å, compared to the spectral width of the sunlight (3000 Å in the visible). Figures 4a and 4b show the results. This reduction in bandwidth yielded a further increase in fringe contrast. From this experiment, it is deduced that radiation which emanates from a large thermal source, such as the sun, can give rise to interference fringes. This experiment demonstrated that the contrast of the fringes from the sunlight radiation and the pinhole separation had some intimate relationship with one another.

When Michelson performed similar experiments on the star Betelgeuse (α-Orionis) with his stellar interferometer,[5] the measured region of spatial coherence was on the order of 3 meters, indicating that the angular subtent of the source determines the size of the region over which interference fringes can be observed.

These results demonstrate that primary incoherent sources give rise to radiation fields which are coherent over small regions of space as determined by their angular subtent and the spectral width of the radiation used in the experiment. The increase of fringe contrast with decreasing pinhole separation and/or bandwidth indicates that the coherence properties of the radiation field are variable and cannot be described by a single number. In fact, the theory of partial coherence relates these fringe variations to different degrees of spatial and temporal coherence which leads to the important concept of a coherence volume. As we will show, the dimensions of this coherence volume become very important in the design of certain classes of instruments.

Historically, these experiments were not fully explained because the high frequency of the complex optical field amplitudes (10^{14}-10^{15} Hz) was and remains beyond the range of existing detectors. Square law detectors, which perform a long-time average, were used to measure the square of the complex field amplitude (intensity). The intensity of the radiation field, which is the measurable quantity, does not satisfy the wave equation, and hence the existing theories were inadequate for explaining the states of partial coherence observed in the Verdet experiment.

The development of the theory of partial coherence circumvented this problem because it was formulated in terms of an observable quantity (the mutual coherence function) which satisfies a pair of coupled-wave equations. The theory includes the effects of polychromatic sources and enables measurement of boundary conditions necessary for the solution of the wave equations.

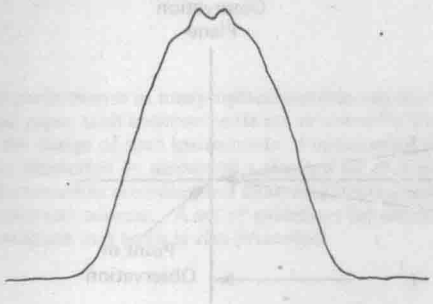

Figure 2 Output of sunlight interferometer experiment and corresponding microdensitometer trace for a pinhole separation of 100 μm. No spectral filter was used in this experiment. (Courtesy of B. Justh)

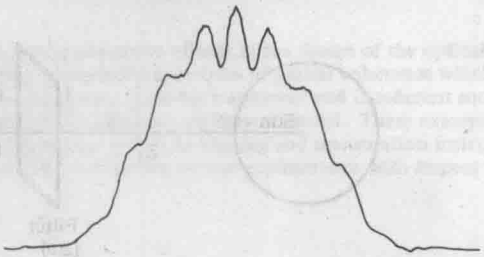

Figure 3 Output of sunlight interferometer experiment and corresponding microdensitometer trace for a pinhole separation of 50 μm. No spectral filter was used in the experiment. (Courtesy of B. Justh)

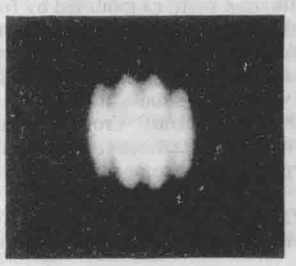

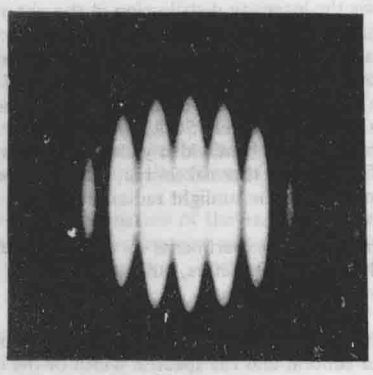

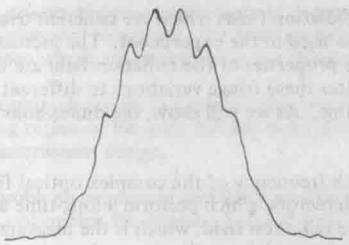

(a)

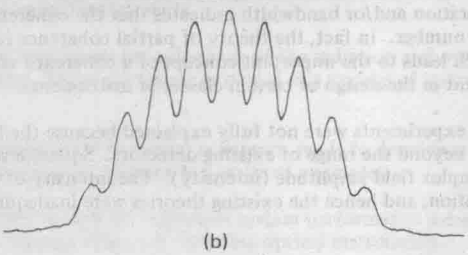

(b)

Figure 4 Output of sunlight interferometer experiment and corresponding microdensitometer traces: (a) 100-μm pinhole with a No. 58 Wratten filter over the pinholes; the filter has a spectral width of approximately 50Å; (b) 50-μm pinhole separation with a No. 58 Wratten filter over pinholes (Courtesy of B. Justh).

Review of the theory of partial coherence*

Introduction

In this section, we examine the two-pinhole experiment using the theory of partial coherence to relate the varying fringe contrast (observed in the sunlight experiment) to the degree of partial coherence of the radiation field. In our approach, we restricted ourselves to the scalar field, and hence we ignored polarization effects. These polarization effects can be readily incorporated into the theory by utilization of the full vector nature of the field.[2,6]

An observable quantity that is measurable is the mutual coherence function introduced by Wolf.[1] This function (of a field assumed to be stationary in time) is defined as a mathematical complex cross-correlation of the optical disturbance at two typical field points, $\bar{x}_1$ and $\bar{x}_2$; that is:

$$\Gamma_{12}(\tau) \equiv \Gamma(\bar{x}_1, \bar{x}_2, \tau) = \langle V_1(\bar{x}_1, t+\tau)\, V_2^*(\bar{x}_2, t)\rangle, \tag{1}$$

where V is the optical disturbance at the point $\bar{x}_1$, V_2 is the optical disturbance at the point $\bar{x}_2$, $\tau = t_2 - t_1$ and is given by $\Delta\ell/c$ (where $\Delta\ell$ is the path difference between the two beams and c is the speed of light in a vacuum), $\bar{x}_n$ denotes a vector quantity, and the angular brackets denote a long time average, i.e.,

$$\langle f(t)\rangle = \lim_{T\to\infty} \frac{1}{2T} \int_{-T}^{T} f(t)\, dt.$$

When the two field points coincide, the cross-correlation becomes an autocorrelation, reducing the mutual coherence function to the self-coherence function which, in turn, reduces to the intensity at the point $\bar{x}_1$ for zero time delay $[I(\bar{x}_1) = \Gamma_{11}(0)]$. The complex degree of coherence is defined as the normalized mutual coherence function:

$$\gamma_{12}(\tau) = \Gamma_{12}(\tau)/[\Gamma_{11}(0)\,\Gamma_{22}(0)]^{1/2}. \tag{2}$$

It should be emphasized that both the modulus and phase of this function are measurable quantities.

In addition, the mutual coherence function in a vacuum also satisfies a pair of coupled-wave equations for propagation; namely:

$$\nabla_n^2 \Gamma(\bar{x}_1, \bar{x}_2, \tau) = 1/c^2 \frac{\partial^2 \Gamma(\bar{x}_1, \bar{x}_2, \tau)}{\partial \tau^2}, \quad n = 1,2 \tag{3}$$

where c is the speed of light and ∇_n^2 is the LaPlacian which operates on the coordinates of the point $\bar{x}_n$. Thus, since the mutual coherence function, in principle, is an optically observable quantity obeying a pair of wave equations, it can be measured on a boundary and specified as a boundary condition. Eq. (3) can then be solved subject to this boundary condition.

Quasi-monochromatic approximation

Consider the system shown in Figure 5a. It is clear that the intensity in the $\bar{x}$-plane depends on the coherence properties of the radiation diffracted at the two pinholes, S_1 and S_2, in the $\bar{\xi}$-plane. It is a simple matter to show that, for the case of partially coherent illumination, the optical disturbances from S_1 and S_2 yield an intensity distribution in the $\bar{x}$-plane at the point P of the form:

$$I_P = |A_1 e^{i\phi_1} + A_2 e^{i\phi_2}|^2 = A_1^2 + A_2^2 + 2\,\mathrm{Re}\,(A_1 A_2^* e^{i(\phi_1 - \phi_2)}), \tag{4}$$

where $A_1 e^{i\phi_1}$ is the diffracted optical disturbance in the $\bar{x}$-plane due to S_1, $A_2 e^{i\phi_2}$ is the diffracted optical disturbance in the $\bar{x}$-plane due to S_2, and Re denotes the real part of a complex quantity. For the case of completely incoherent illumination, the intensity at the point P is given by

$$I_P = A_1^2 + A_2^2 = I_1 + I_2, \tag{5}$$

where I_1 and I_2 are the intensities at P due to S_1 and S_2, respectively. For the completely coherent case, as well as the general partially coherent case, the intensity in the $\bar{x}$-plane is given by Eq. (4). The cross term in Eq. (4) is the distinguishing and important term to be considered. Although Eqs. (4) and (5) describe the principle of the interference phenomena, we must return to the coherence theory formulation for a rigorous mathematical description of this experiment.

The quasi-monochromatic form of coherence theory is characterized by the condition that the spectral width of the radiation ($\Delta\nu$) is taken to be very small compared to the mean frequency (ν'):

$$\Delta\nu \ll \nu'. \tag{6}$$

If in addition we assume that all path differences satisfy the condition:

$$\Delta\ell \ll c/\Delta\nu, \tag{7}$$

*This section closely follows the development in Chapter 3 of the "Theory and Application of Holography" by J.B. DeVelis and G.O. Reynolds, Addison-Wesley Publishing Company (1967).

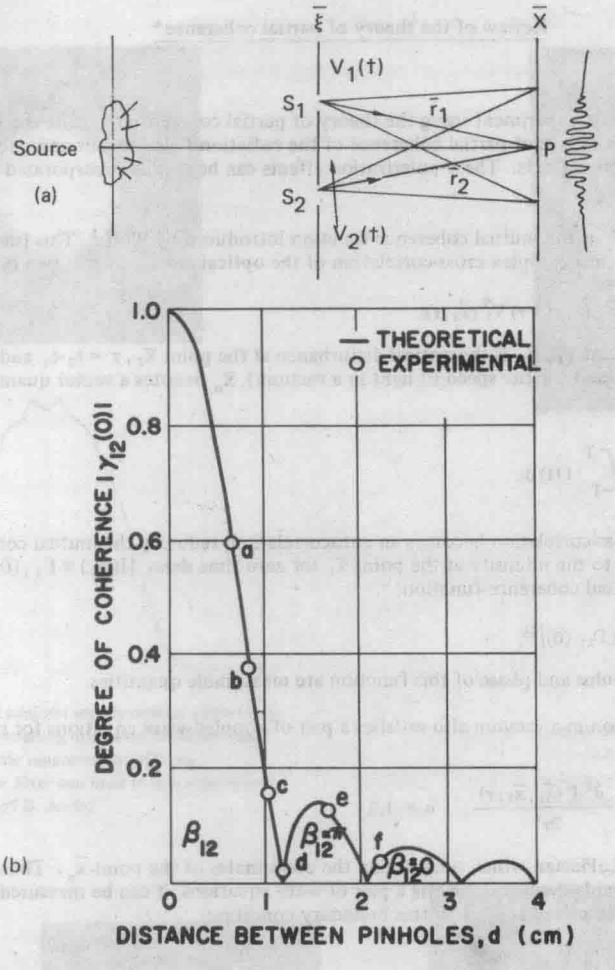

Figure 5 Measurement of modulus of complex degree of coherence: (a) schematic for two-pinhole experiment where P denotes a general point of observation in the $\bar{x}$ - plane; (b) modulus of complex degree of coherence as a function of pinhole separation for the experimental arrangement shown in figure (5a) where phase change $\beta_{12} = 0$ and π. (a) from reference (2); (b) from reference (1).

then the radiation behaves much as if it were monochromatic of frequency ν'. Thus, the second condition (Eq. 7) puts a strong restriction on all path differences to which this theory is applied. Since the approximations given by Eqs. (6) and (7) are assumed here, the details of the spectral composition of the light may be ignored, and all frequency-dependent parameters may be evaluated at the mean frequency, ν'.

In Figure 5(a), S_1 and S_2 are two quasi-monochromatic sources, and $V_1(t)$ and $V_2(t)$ are stationary random functions which describe the light oscillations at S_1 and S_2. The conditions under which the results given above are valid can now be considered. Since the light disturbances are propagated by linear differential wave equations, the disturbance at P may be represented as a superposition of the contributions from S_1 and S_2 in the form:

$$V_P(t) = K_1 V_1 (t - r_1/c) + K_2 V_2 (t - r_2/c), \tag{8}$$

where K_1 and K_2 are propagators, and r_1 and r_2 are the distances from P to S_1 and S_2, respectively.

The intensity at P is then given by

$$I(P) = \langle V_P(t) V_P^*(t) \rangle. \tag{9}$$

Equation (9) may be rewritten as

$$I(P) = \langle | K_1 V_1(t - r_1/c) + K_2 V_2(t - r_2/c) |^2 \rangle = I_1 + I_2 + 2 \, \mathrm{Re} \left\{ K_1 K_2^* \langle V_1(t - r_1/c) V_2^*(t - r_2/c) \rangle \right\}, \tag{10}$$

where I_1 and I_2 are the intensities at P due to S_1 and S_2. Note the similarity between this result and that stated in Eq. (4). Because of the time invariance, the term inside the angular brackets depends only on $r_1/c - r_2/c = \tau$ and not on r_1/c and r_2/c explicitly. Thus, the origin of time can be changed and Eq. (10) can be rewritten:

$$I(P) = I_1 + I_2 + 2\,\mathrm{Re}\left\{K_1 K_2^* \Gamma_{12}(\tau)\right\}, \tag{11}$$

where Γ_{12} is described by Eq. (1). Since only quasi-monochromatic light is being considered, the experiment is restricted to small path differences defined by Eq. (7). For this case, we form the function $\Gamma_{12}(0)$, which is termed the mutual intensity function. Furthermore, because K_1 and K_2 are purely imaginary, the notation:

$$\Gamma_{12}(\tau) = |\Gamma_{12}(0)|\, e^{i\Phi_{12}} \equiv |\Gamma_{12}|\, e^{i\Phi_{12}}$$

is introduced, where $\Phi_{12} = 2\pi\,\nu'\,\tau + \beta_{12}$, $2\pi\,\nu'\,\tau$ = phase difference = $(2\pi/\lambda')\,(|\bar{r}_1 - \bar{r}_2|)$ (12)

and $\beta_{12} = \arg\,[\,\Gamma_{12}(\tau)]$.

[For a further discussion of this point, see Refs. (1, 2).]

Eq. (11) can be rewritten as

$$I(P) = I_1 + I_2 + 2\,|K_1 K_2^*|\,|\Gamma_{12}|\cos\Phi_{12}. \tag{13}$$

Using Eq. (2), we can rewrite Eq. (13) as

$$I(P) = I_1 + I_2 + 2\sqrt{I_1 I_2}\,|\gamma_{12}|\cos\Phi_{12}. \tag{14}$$

Eq. (14) is the generalized interference law for partially coherent quasi-monochromatic light. For the case of incoherent light, $|\gamma_{12}| = 0$, and Eq. (14) becomes:

$$I(P) = I_1 + I_2, \tag{15}$$

which is the result given by Eq. (5), and states that there is no interference, as expected, since incoherent light was assumed to superimpose in intensity. For the case of coherent radiation, $|\gamma_{12}| = 1$, and Eq. (14) becomes:

$$I(P) = I_1 + I_2 + 2\sqrt{I_1 I_2}\,\cos\Phi_{12}, \tag{16}$$

which is the well-known interference law for coherent radiation. For the case of intermediate values of $|\gamma_{12}|$, the radiation is termed partially coherent and the resulting interference is governed by Eq. (14).

A qualitative description of some basic experiments which illustrate coherence effects can now be given. It should be emphasized again that the effects of coherence in a radiation field are all contained in the complex function $\gamma_{12}(\tau)$. However, as an aid in understanding coherence principles, it is useful to separate coherence effects into two categories. The first, termed spatial coherence, arises primarily from angular source size considerations, and the second, termed temporal coherence or coherence length, arises from considerations of the finite spectral width of the radiation. Thus, $\gamma_{12}(0)$ measures spatial coherence effects and $\gamma_{11}(\tau)$ is a measure of temporal coherence. In general, the two-pinhole experiment discussed in deriving Eq. (14) is used for measuring spatial coherence effects. To isolate this effect we demand $|\bar{r}_1 - \bar{r}_2| \ll \Delta\ell$ where $\Delta\ell$ was defined in Eq. (7).

To illustrate an important technique for measuring the spatial coherence between two disturbances, we shall consider Eq. (14) where $I_1 = I_2 = I$.

Eq. (14), then reduces to

$$I(P) = 2\,I\,(1 + |\gamma_{12}|\cos\Phi_{12}), \tag{17}$$

(that is, an interference pattern with reduced visibility is observed).

If the visibility of the fringes, V, is defined as

$$V = \frac{I_{max} - I_{min}}{I_{max} + I_{min}}, \tag{18}$$

and if we then use this equation to compute the visibility of the fringes described by Eq. (17), the resulting visibility becomes:

$$V = |\gamma_{12}| \tag{19}$$

Eq. (19) demonstrates the relationship between the modulus of the complex degree of coherence and the fringe visibility for this experiment. The phase of the complex degree of coherence is related to the relative position of the central fringe to the origin when the pinholes are symmetrically displaced with respect to the optical axis. To measure the degree of spatial coherence between two disturbances, their intensities are adjusted to be equal, and the visibility of the resulting fringes is measured by allowing them to interfere. A typical curve demonstrating the variation of the modulus of the complex degree of coherence as a function of pinhole separation is shown in Figure 5(b). In this figure the solid line represents the theoretical value and the designated points are the experimental values quantitatively described in

Figure 6. Figures 6 and 7 show a comparison of the experimental and theoretical results, demonstrating the effects of fringe visibility and the corresponding phase shifts in Φ_{12}, given by Eq. (17), which arise from a distant incoherent source.[7,8] The theoretical coherence function in this case is calculated by utilizing the Van Cittert-Zernike theorem[1,2] which will be derived later. In Figure 6, the fringe visibility was varied by changing the separation distance between the pinholes in a two-pinhole interference experiment, and in Figure 7 the degree of spatial coherence was changed by varying the size of the pinhole in a collimator.

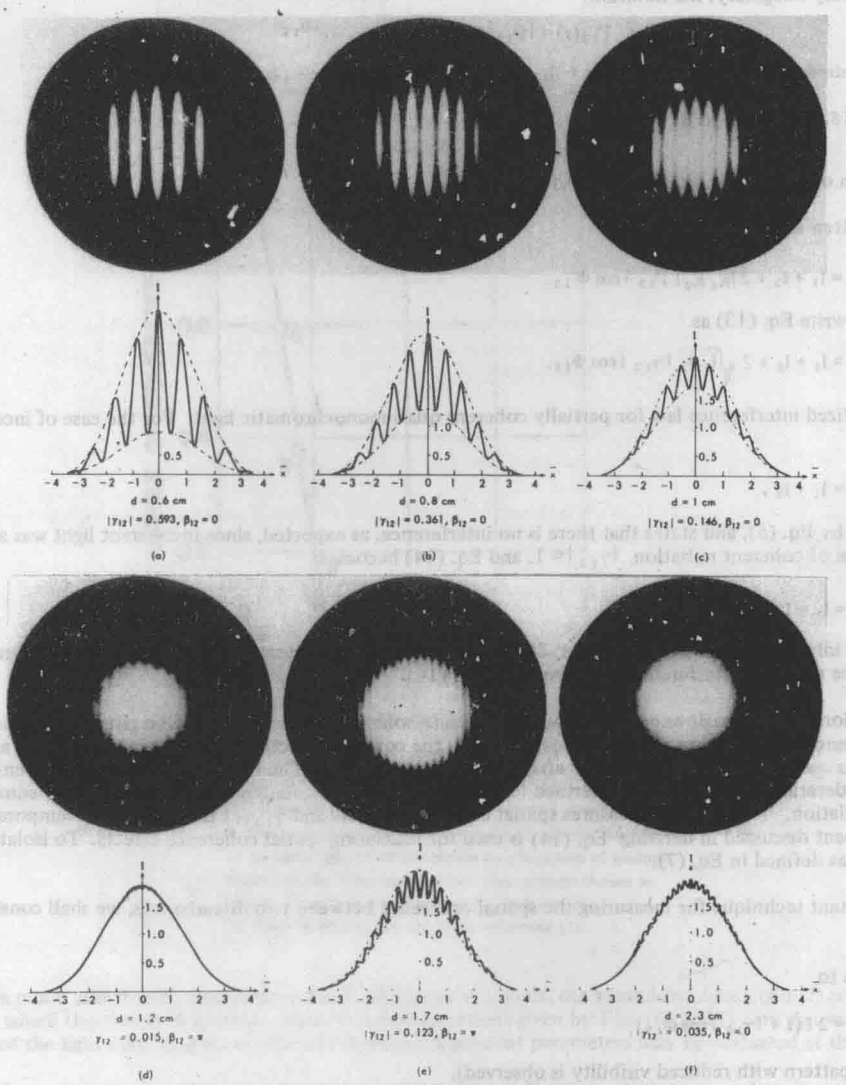

Figure 6 **Two-beam interference experiment utilizing partially coherent light and exhibiting spatial coherence effects. The upper portion of (a) through (f) shows fringe visibility patterns; the lower portion, theoretical intensity curves where the dashed lines represent the values of maximum and minimum intensity. In these experiments, the fringe visibility and frequency were varied by changing the separation distance d between the pinholes. Figures (a) through (c) show the decrease in fringe visibility and corresponding increase in frequency as the separation distance between the two pinholes increases; (d) and (e) show a phase shift $\beta = \pi$ in the fringe pattern with respect to the origin and the resulting fringe visibility and increased frequencies for two additional separation distances. Figure (f) shows another π-phase shift resulting in a maximum intensity at the origin and corresponding fringe visibility and increased frequency due to further separation of the pinholes. Figures (a) through (c) correspond to points on the first lobe $|\gamma_{12}|$; figures (d) and (e), to points on the second lobe; and figure (f), to a point on the third lobe in Figure 5-b (from reference 8).**

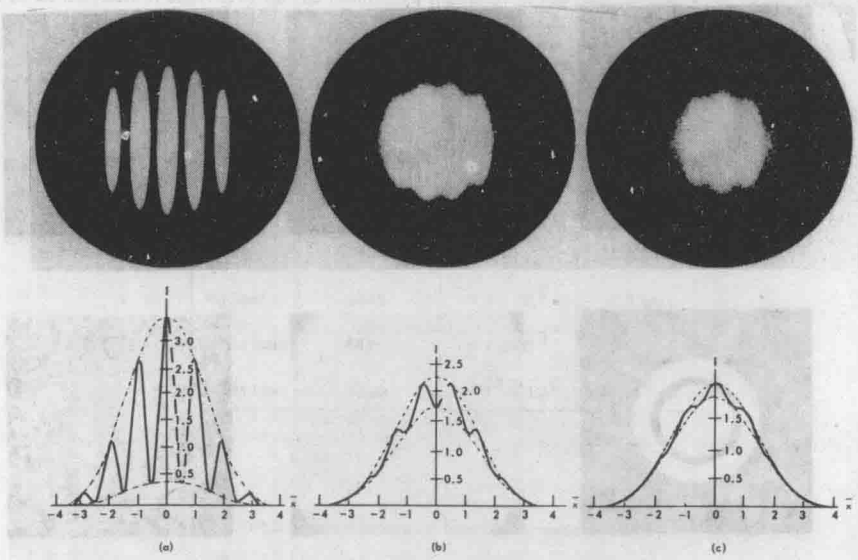

Figure 7 **Two-beam interference experiment utilizing partially coherent light, showing change of phase and exhibiting spatial coherence effects. The upper portion of (a) through (c) shows the observed patterns; the lower portion, the theoretical intensity curves where the dashed lines represent the maximum and minimum intensities. In these experiments the pinhole separation was fixed so that the resulting fringe frequency was constant. The degree of coherence at the two pinholes was varied by changing the size of the primary incoherent source used in the experiment and is illustrated by the different fringe visibilities in (a) through (c). The π-phase shift apparent from examining the central fringe of these figures results from sampling different lobes of the coherence function at the pinhole plane (from reference 7).**

The qualitative effect of temporal coherence (coherence length) and an example demonstrating the validity of the quasi-monochromatic approximations [Eqs. (6) and (7)] is shown in Figure 8. In one of these experiments, Figure 8(a-d), path lengths were varied by placing different thicknesses of optically flat glass in front of one of the pinholes and illuminating the interferometer with both laser light and filtered collimated thermal light. The thickness of the glass was chosen to exceed the coherence length of the thermal light, but not that of the laser light. In the other experiment, Figure 8(e,f), the radiations were chosen so that the surface irregularities were greater in depth than the coherence length of one source but not the other, the result being a loss of interference in the former case. The experiments presented in Figure 8 demonstrate the importance of the quasi-monochromatic approximation and the necessity of an experiment to measure temporal coherence effects [that is, $|\gamma_{11}(\tau)|$]. One experiment for measuring $\gamma_{11}(\tau)$ is a Michelson interferometer with a path length compensator in one arm.[1,2] In such an experiment, a beam splitter is used to divide the quasi-monochromatic radiation into two separate beams which are recombined after one of them is passed through a compensator to adjust the optical path length. The fringe visibility, given by Eq. (18), at the observation point is varied by moving one of the mirrors until the fringes disappear.

Coherence volume

One interpretation of the results of the two-pinhole experiment gives rise to the concept of the coherence volume. The coherence volume defines a region of space, in any given experiment, for which radiation from any pair of points within the volume will interfere. Similarly, radiation emanating from points separated by distances larger than those defined by the dimensions of the coherence volume will not interfere. The two-pinhole experiment described a lateral dimension of the incoming wave field for which interference fringes were observed. This dimension is called the spatial coherence interval. The spectral bandwidth experiments indicated a maximum longitudinal dimension of the incoming wave field over which interference effects could be observed. We call this maximum length $\Delta\ell$, as defined by the equality in Eq. (7), the "coherence length" of the radiation field.

Both spatial and temporal coherence dimensions are characterized by gradual rather than sharp changes in fringe contrast, as seen in Figure 5(b) for the case of spatial coherence. These two characteristic dimensions of "spatial coherence" and "temporal coherence" length define a "coherence volume" for the radiation field, as shown schematically in Figure 9. In Figure 9, we see a representation of the "coherence volume" whose characteristic area normal to the direction of propagation is determined by the maximum value of the spatial coherence (C.I.), and whose third-dimension along the direction of propagation of the wave is determined by $\Delta\ell$, the coherence length of the radiation.

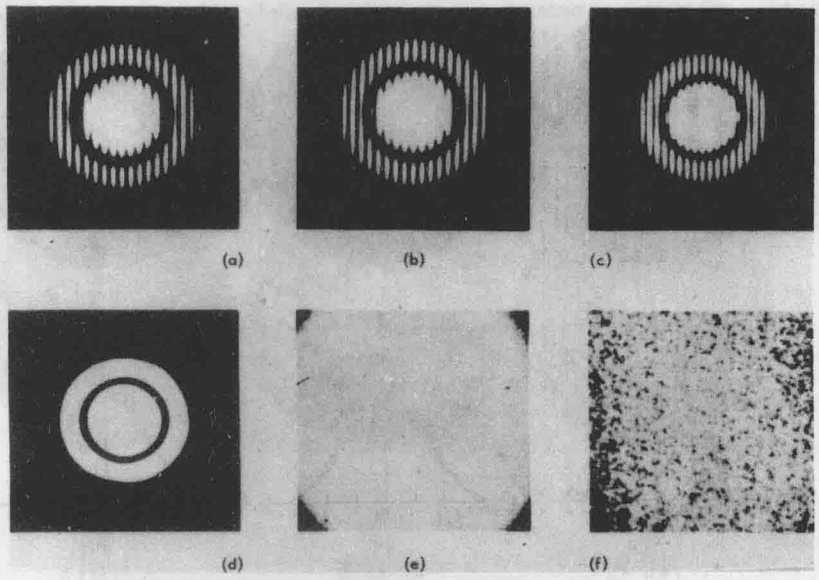

Figure 8 Two-beam interference experiment utilizing partially coherent light and exhibiting temporal coherence effects. Figure (a) shows high-contrast fringes formed with a He-Ne gas laser illuminating a pair of small circular apertures. In (b) a piece of plain optical-quality glass, 0.5 mm thick, was introduced in front of one of the apertures to add an extra optical path. Again illuminating with He-Ne gas laser, no difference in the fringe contrast is observed. Figure (c) shows high-contrast fringes when the experiment is repeated with a coherent field produced by a collimated mercury arc lamp without the glass plate; however, with the glass in place the fringes disappear as shown in (d). (The scale change between the two pairs of illustrations is due to different wavelengths: 6328 Å for He-Ne and 5461 Å for Hg). Figures (e) and (f) are photographs of a cement block illuminated with a collimated mercury arc lamp and a He-Ne gas laser, respectively. Both illuminating fields have approximately the same degree of spatial coherence, but the laser has a coherence length greater than the depth of roughness on the surface of the block. The absence of speckling in (e) allows one to see the surface structure (from reference 9).

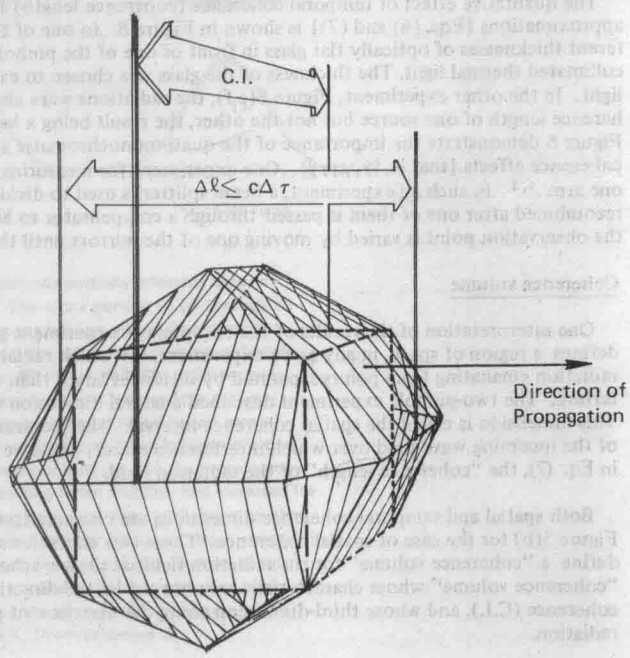

Figure 9 Schematic of coherence volume whose length $\Delta\ell$ is determined by the temporal coherence and whose cross-sectional area is determined by the spatial coherence interval, C.I. The transitional region (shaded areas) is not sharp because the fringe visibility gradually goes to zero as indicated in Fig. 5b for the case of spatial coherence.